Cureus Journal of Engineering

Open Access Original Article

An Analytical Investigation on Chemical, Structural, and Relative Distribution of Minerals in Mineralogical Cores

Murugesan Sugumaran [1] , Gayathri Arun [1]

1. Department of Physics, Sathyabama Institute of Science and Technology, Chennai, IND

Corresponding author: Murugesan Sugumaran, binunair.phd@gmail.com

Received 06/29/2025
Review began 07/13/2025
Review ended 07/29/2025
Published 09/08/2025

DOI:
https://doi.org/10.7759/s44388-025-08584-w

Abstract

This study investigates the mineralogical and geochemical characteristics of rock samples collected from Perumbakkam, Tamil Nadu, using Fourier Transform Infrared Spectroscopy (FTIR) and X-ray Diffraction (XRD). Quartz was identified as the dominant mineral (35-52wt%) in most samples, with orthoclase (in sites N4, S4, and E3) being dominant where quartz content was lower. FTIR spectra confirmed the presence of silicates, iron oxides, clay minerals, carbonates, and organic matter. Crystallinity index values of quartz remained <1 across all samples, indicating well-ordered crystalline structure. The highest crystallinity was noted at 60 feet depth (90.55%) and the lowest at 160 feet (12.81%). Extinction coefficients of quartz ranged from 528.01 to 790.36, with mountain samples showing a broader distribution of minerals including halloysite. The rock samples showed alkaline pH values ranging from 7.15 to 7.50. Bacterial counts varied from 1.2×10^5 to 3.6×10^6CFU/g, supporting microbiological viability and soil fertility. The integrated FTIR-XRD analysis, coupled with pH and microbial data, highlights the region's suitability for agricultural use and ecological sustainability.

Categories: Environmental and Sustainable Engineering, Environmental Engineering
Keywords: x-ray diffraction, ftir, quartz, minerals, crystallinity index

Introduction

Rocks are essential components of the Earth's crust, supporting both geological processes and human activities. Rocks are solid masses of natural origin with one or more minerals, which acquire their classification through mineral content analysis as well as formation methods and chemical makeups [1]. There exist three principal types of rocks, which include igneous rocks and sedimentary rocks and metamorphic rocks. The creation of igneous rocks results from solidification followed by cooling of molten material, while sedimentary rocks form through sediment deposition followed by compaction yet metamorphic rocks develop when previously formed rocks change high temperature and pressure conditions [2]. Rocks possess distinct physical and chemical properties that determine their resistance, permeability, and suitability for environmental and industrial applications.

All rocks contain silicate minerals as their main composition along with oxides, carbonates, sulfides, and phosphates. The essential rock-forming minerals include quartz, feldspar as well as micas, amphiboles and pyroxenes and olivine together with clay minerals. The study of rock-forming minerals delivers mechanical power and weathering capacity to rocks so builders and natural resource explorers and environmental protectors find this subject essential [3-5]. Geological region history assessment along with mineral resource aid depends on rock mineralogical analysis as an essential practice.

The combination of contemporary analytical techniques including X-ray Diffraction (XRD) and Fourier Transform Infrared Spectroscopy (FTIR) provides better options for rock composition analysis. XRD represents an extensively utilized technique for mineral phase identification and sample geological mineral content determination. XRD produces diffraction patterns for individual minerals through the interaction of X-rays with crystal structures based on Bragg's Law principles [6]. XRD works most effectively to identify minerals present in fine-grained samples, which are inaccessible through routine microscopic analysis. Modern investigations use XRD technology to evaluate geological structures while determining rock mineral contents for scientific and business applications.

FTIR spectroscopy serves as a mineralogical analysis method to detect functional groups by analyzing their molecular vibrations. Rock materials benefit from this method for detecting clay minerals together with carbonates and organic molecules. Infrared radiation absorbance detection by different mineral structures in FTIR produces spectral patterns that characterize sample chemical compositions [7-9]. Modern improvements in FTIR technology created more sensitive identification processes for minerals and made the instrument indispensable for environmental research and geochemical investigations.

This study focuses on the mineralogical characterization of rock samples collected from Perumbakkam

Hill, Tamil Nadu, India, using advanced analytical techniques, namely XRD and FTIR. The primary objective is to identify major and accessory minerals and to evaluate the structural and chemical composition of the samples. These analyses are relevant for applications in geological exploration, materials science, and environmental assessment. By integrating modern mineralogical methods with recent scientific advancements, the study provides a comprehensive dataset that contributes to evaluating the suitability of Perumbakkam Hill rocks for construction, industrial utilization, and sustainable resource management.

Materials And Methods

Location and geology

The suburban region of Perumbakkam exists in Chennai municipality along Tamil Nadu's coast with its location within Chengalpattu district at 12.9053°N and 80.1986°E degrees. The total area of Perumbakkam amounts to 5.88 square kilometers with Sholinganallur and Semmencherry on one side and Medavakkam and Sithalapakkam on the other. The region has a tropical wet and dry climate while its seasons show minimal changes [10]. Within the growing IT hub region, Perumbakkam maintains its ecological value as part of the Eastern Ghats ecosystem [11].

This natural area hosts many species as dry deciduous forests and scrubland areas, and grasslands create essential habitats for wildlife [12]. The hill maintains its dual value between environmental conservation and recreational use through hiking trails and nature walks which bring visitors from local residents to tourists. The area's biodiversity, together with natural resources, faces risks as urban growth continues progressively. Environmental organizations together with local authorities use sustainable land-management practices to lessen negative impacts on the area under their leadership.

Research has adopted Perumbakkam hill as its study area given its dual significance in geology and environmental science. Figure *1* present the locator map which describes the study area location.

FIGURE 1: Geographical location of the study area (Perumbakkam hill)

Sample collection and preparation

The extraction of rock samples using percussion drilling techniques was performed at Perumbakkam hill throughout multiple depths ranging from 60 to 170 feet with measurements at 20-foot intervals (60, 80, 100, 120, 140, 160, and 170 feet). The sampling campaign began at 60 feet because initial soil and regolith assessments indicated that the upper 60 feet mainly comprised weathered overburden and loose sediments with inconsistent lithology. These superficial layers were excluded from detailed mineralogical analysis due to poor core recovery and limited mineral structure. The depth range of 60 to 170 feet was selected to investigate geologically stable, consolidated rock zones known to exhibit mineralogical variation. These depths capture the transition from partially weathered rock to unweathered bedrock. Sampling at 20-foot intervals ensured sufficient vertical resolution to detect mineralogical trends while optimizing drilling efficiency and sample representativeness. Extreme dryness at room temperature,

followed by sample homogenization, led to sieving for examination purposes. The success of accurate analysis depended on carrying out proper sample preparation. A clean shovel was used to avoid contamination and sampling happened at key locations to deal with spatial differences. The samples received clean, labeled storage containers before being put in a closed space under cool dry conditions out of sunlight exposure. The specimens underwent two-stage drying at room temperature followed by the hot air oven operated at 105°C to dry out the moisture content for microbial inactivity prevention. After drying, the samples received systematic powdering with a mortar and pestle to achieve better homogeneity and maximize analysis surface area. The manufacturers carried out ASTM standard sieve procedures to process the powdered samples through a 1-mm mesh to obtain consistent results. The selected sieved material was properly mixed before being stored in specially identified containers to prevent contamination during testing periods.

X-Ray Diffraction (XRD) analysis

Laboratory testing for mineralogical analysis occurred at the Advanced Studies Laboratory of Sathyabama University, Chennai, through the utilization of an ARL EQUINOX3000 X-ray diffractometer. The analyzed range of diffraction angles (2θ) included values from 0 to 80º for crystalline phase evaluation in the samples. The Joint Committee on Powder Diffraction Standards (JCPDS) data together with intensity measurements and d-spacing values served for mineral identification [13]. A complete table included values for relative intensities coupled with d-spacing data and 2θ angles, which led to the identification of minerals within the samples.

Rock samples were obtained from different depths (60, 80, 100, 120, 140, 160, and 170 feet) at Perumbakkam hill using percussion drilling. The collected samples were air-dried at room temperature, homogenized, and sieved for further examination. To obtain precise analysis results, proper sample preparation techniques had to be followed. A clean shovel served as the sampling instrument while representatives of each area were selected to monitor location variation. Laboratory staff stored the samples under conditions with shade and cool temperatures and dryness in labeled sanitary containers. Surface moisture from the samples was removed by drying them at room temperature on trays. The samples were dried in a hot air oven set to 105°C to eliminate both moisture content and microbial activity. The samples went through a drying process before being ground as a fine powder through mortar and pestle grinding to enhance analysis conditions. The powdered samples were then passed through a 1-mm mesh sieve by ASTM standards to ensure uniformity. We chose a portion of the sieved material, followed by extensive mixing to ensure sample consistency before placing it in labeled containers for storage before additional tests.

Fourier Transform Infrared Spectroscopy (FTIR)

The FTIR spectra analysis occurred with a Perkin Elmer Spectrum Two spectrometer found at the Archbishop Casimir Instrumentation Centre (ACIC) at St. Joseph's College, based in Tiruchirappalli, Tamil Nadu. A Kimaya Engineers 15-ton hydraulic press managed KBr pellet production through the combination of rock powder and KBr in equal weight proportions of 1:10. Measurement of absorption bands occurred from 4000 cm^{-1} to 400 cm^{-1} during spectral recording. The instrument operated with a precision of ±5 cm^{-1}, which delivered accurate mineral composition analysis.

The pour plate approach

Sterilized collection containers and sterile conditions were used for the rock sampling procedure. Bacterial viability was assessed using the pour plate method in conjunction with Colony-Forming Unit (CFU) tests. Serial dilutions were required to achieve an accurate colony count. A milliliter of diluted solution was added to Petri dishes with dilution factor information prior to the introduction of sterile agar by a laboratory worker. Up to 20 milliliters of sterile, cooled agar medium were added to each plate, and the medium was gently swirled to ensure even distribution [14]. Throughout the agar solidification process, the researcher kept the plates at room temperature. In their apparatus, Hotking Instruments incubated the solidified plates for 24 hours at 37°C. Following the conclusion of the incubation period and the recording of the results, the developed colonies were counted to calculate the CFU values.

pH measurement

The Susima-Minimax pH meter served to determine the pH values in rock samples. The combination of one gram of rock powder crushed to fine particles and 10 milliliters of distilled water in a clean beaker formed a suspension through continuous stirring. During 1 hour of undisturbed mixture exposure, the researcher stirred the container periodically to promote contact between water and rock material. A suspension did not move when the electrode of the pH meter was placed inside and a readout was taken. Before experimentation, the distilled water pH measurement served as the control for accuracy purposes [15]. The experimental team refrained from using tap water to stop accidental contamination during the analysis process. The combination of appropriately prepared samples together with analytical methods achieved exact assessment results for both mineralogical and microbial composition, along with chemical analysis of rocks gathered from Perumbakkam hill.

Use of Large Language Models (LLMs) including Artificial Intelligence (AI)

Large Language Models (LLMs), specifically OpenAI's ChatGPT, were used to assist with language refinement, grammar improvement, and formatting clarity during manuscript preparation. The authors solely conducted the scientific content, data interpretation, and analysis. The AI tool did not generate any original research content, results, or conclusions. All factual statements were cross-verified by the authors to ensure accuracy and reliability. No AI tools were used for data analysis, figure generation, or experimental design. The final manuscript was thoroughly reviewed and edited by the authors to ensure that all content meets academic standards and reflects original intellectual work.

Results And Discussion

XRD analytical results

XRD has emerged as a highly effective technique for both qualitative and quantitative analysis of geological samples. Numerous scientific publications have elaborated on its applications in mineral identification and compositional assessment [16,17]. The results of the rock sample analysis conducted in this study are systematically presented in Table *1*, while the corresponding X-ray diffractograms are illustrated in Figures *2* and 3. The mineralogical composition was determined through XRD analysis, based on the principles of Bragg's law. References such as the book by Sachinath Mitra and other related literature were consulted to interpret the diffractograms [18-21]. The obtained XRD patterns were compared with standard data from the JCPDS. The tabulated data include values for position (2θ), d-spacing (Å), and mineral identification, whereas the figures visually represent the diffraction patterns of these minerals. This study employs XRD analysis to determine the presence of major, minor, and trace minerals in the rock samples. The diffraction patterns confirm that for every 2θ value, an associated intensity peak is observed-an essential criterion for estimating mineral percentages [22]. The mineral composition can be quantified using the following formula:

$$[\text{Mineral Percentage} = \left(\frac{\text{Intensity of the Peak}}{\text{Total Intensity of All Peaks}}\right) \times 100]$$

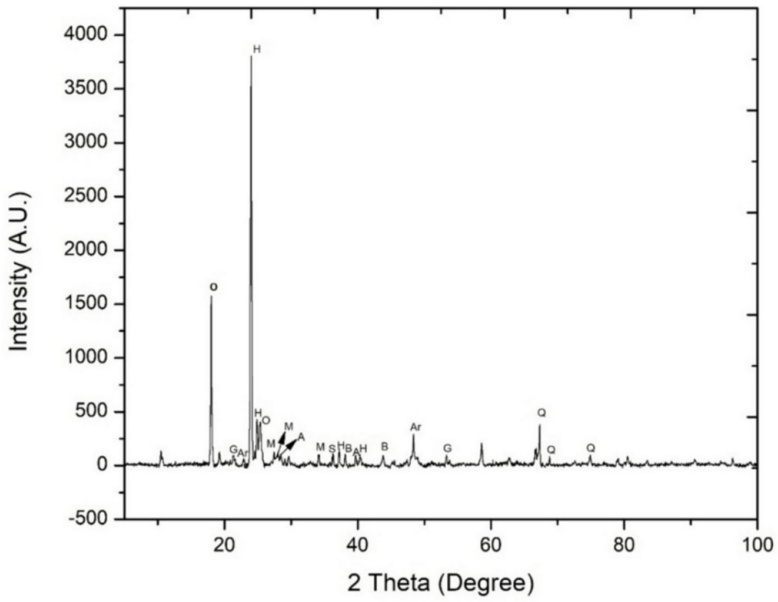

FIGURE 2: Representative X-Ray Diffraction spectrum for 60 feet depth

The proportion of each mineral is determined by analyzing the peak intensities in the XRD data. Each mineral is identified based on its characteristic 2θ value and corresponding intensity. To ensure accurate identification, minerals are matched to their respective 2θ values. Quartz is the predominant mineral at most depths, except at 60, 120, and 170 feet, where hematite is dominant.

Sl. No.	Pos. [°2Th.]	Minerals	%	Depth	Sl. No.	Pos. [°2Th.]	Minerals	%	Depth	Sl. No.	Pos. [°2Th.]	Minerals	%	Depth	Sl. No.	Pos. [°2Th.]	Minerals	%	Depth
1	75.2	Arago	0.97	170	34	14.11	Bauxite	0.76	100	67	67.15	Hematite	3.1	120	100	25.95	Orthoclase	6.87	140
2	48.37	Arago	2.87	60	35	28.48	Bauxite	1.15	120	68	23.95	Hematite	2.3	140	101	30.16	Orthoclase	2.23	140
3	22.91	Arago	0.66	60	36	43.96	Bauxite	1.6	120	69	36.02	Hematite	1.24	140	102	29.95	Orthoclase	3.14	160
4	22.09	Arago	1.54	80	37	28.36	Bauxite	9.91	140	70	23.92	Hematite	4.96	160	103	18.04	Orthoclase	9.2	170
5	23.42	Arago	1.06	80	38	39.87	Bauxite	1.58	140	71	24.68	Hematite	3.51	160	104	25.42	Orthoclase	19.02	170
6	49.41	Arago	0.65	80	39	43.02	Bauxite	1.04	160	72	35.93	Hematite	3.24	160	105	27.96	Orthoclase	2.03	170
7	22.33	Arago	1.28	100	40	38.36	Bauxite	2.38	170	73	23.03	Hematite	2.39	170	106	50.65	Quartz	6.8	100
8	23.56	Arago	1.28	100	41	43.99	Bauxite	1.17	170	74	24.13	Hematite	35.29	170	107	50.68	Quartz	3.86	140
9	32.43	Arago	1.24	100	42	21.32	Goethite	0.9	60	75	40.5	Hematite	2.67	170	108	50.65	Quartz	1.25	160
10	22.97	Arago	1.85	120	43	53.32	Goethite	2.12	60	76	58.68	Hematite	2.49	170	109	68.78	Quartz	0.95	60
11	48.46	Arago	4.79	120	44	21.03	Goethite	7.99	80	77	28.1	Microcline	5.92	80	110	67.31	Quartz	3.96	60
12	48.92	Arago	1.77	120	45	21.09	Goethite	5.47	100	78	27.47	Microcline	1.16	60	111	74.9	Quartz	0.94	60
13	22.3	Arago	8.68	140	46	20.95	Goethite	3.29	120	79	28.02	Microcline	1.1	60	112	26.86	Quartz	25	80
14	32.54	Arago	1.33	140	47	53.78	Goethite	1.34	120	80	34.23	Microcline	0.99	60	113	46.03	Quartz	1.08	80
15	22.24	Arago	4.68	160	48	21.09	Goethite	4.59	140	81	27.8	Microcline	7.52	80	114	68.49	Quartz	3.61	80
16	49	Arago	2.87	160	49	21.15	Goethite	2.99	160	82	34.55	Microcline	0.7	80	115	76.38	Quartz	0.66	80
17	48.49	Arago	3.65	170	50	21.16	Goethite	2.8	170	83	55.54	Microcline	0.79	80	116	26.95	Quartz	28.48	100
18	28.45	Augite	0.89	60	51	24.01	Hematite	41.9	60	84	27.75	Microcline	5.69	100	117	68.78	Quartz	3.85	100
19	39.71	Augite	1.12	60	52	24.9	Hematite	4.39	60	85	42.38	Microcline	1.37	100	118	76.26	Quartz	1.12	100
20	28.33	Augite	6.02	80	53	37.23	Hematite	1.76	60	86	55.6	Microcline	3.82	100	119	20.18	Quartz	1.17	120
21	39.79	Augite	2.1	80	54	40.38	Hematite	0.97	60	87	34.2	Microcline	2.21	120	120	58.71	Quartz	2.59	120
22	28.36	Augite	10.76	100	55	24.33	Hematite	0.99	80	88	28.07	Microcline	9.85	140	121	26.98	Quartz	21.14	140
23	39.9	Augite	2.39	100	56	24.98	Hematite	0.95	80	89	34.28	Microcline	0.45	140	122	46.38	Quartz	1.41	140
24	28.2	Augite	0.73	120	57	35.58	Hematite	1.03	80	90	42.35	Microcline	2.77	140	123	60.78	Quartz	1.61	140
25	39.83	Augite	1.42	120	58	37.08	Hematite	1.33	80	91	55.51	Microcline	0.68	140	124	68.61	Quartz	2.93	140
26	28.6	Augite	4.47	140	59	40.79	Hematite	1.26	80	92	42.85	Microcline	2.27	160	125	26.98	Quartz	43.95	160
27	28.36	Augite	9.51	160	60	24.27	Hematite	1.37	100	93	34.26	Microcline	2.2	170	126	60.51	Quartz	1.84	160
28	39.9	Augite	2.44	160	61	35.81	Hematite	1.03	100	94	18.01	Orthoclase	16.94	60	127	68.99	Quartz	0.89	160
29	28.6	Augite	2.17	170	62	36.99	Hematite	3.93	100	95	25.39	Orthoclase	4.49	60	128	78.41	Quartz	2.76	160
30	43.38	Bauxite	2.67	140	63	40.82	Hematite	1.62	100	96	25.86	Orthoclase	1.6	80	129	67.12	Quartz	6.27	170
31	38.12	Bauxite	1.15	60	64	24.07	Hematite	33.11	120	97	25.89	Orthoclase	2.04	100	130	36.31	Quartz	2.5	60
32	43.84	Bauxite	0.99	60	65	37.35	Hematite	2.49	120	98	18.01	Orthoclase	6.22	120					
33	42.91	Bauxite	1.48	80	66	40.44	Hematite	0.98	120	99	25.29	Orthoclase	12.33	120					

TABLE 1: Mineral identification and distribution for various sampling sites

The identification of mineral phases through XRD relies heavily on the recognition of characteristic peak positions and their corresponding d-spacing values. While the presence of two or three prominent peaks may initially suggest a particular mineral, such limited data can often lead to misidentification, especially

in complex or mixed-phase samples. Therefore, a comprehensive evaluation of the entire diffraction pattern, supported by a detailed analysis of d-spacing values, becomes essential for accurate phase determination. Furthermore, variations in diffraction patterns among different structural or polymorphic forms of the same mineral highlight the diagnostic value of subtle d-spacing shifts, reinforcing their importance in resolving mineralogical ambiguities.

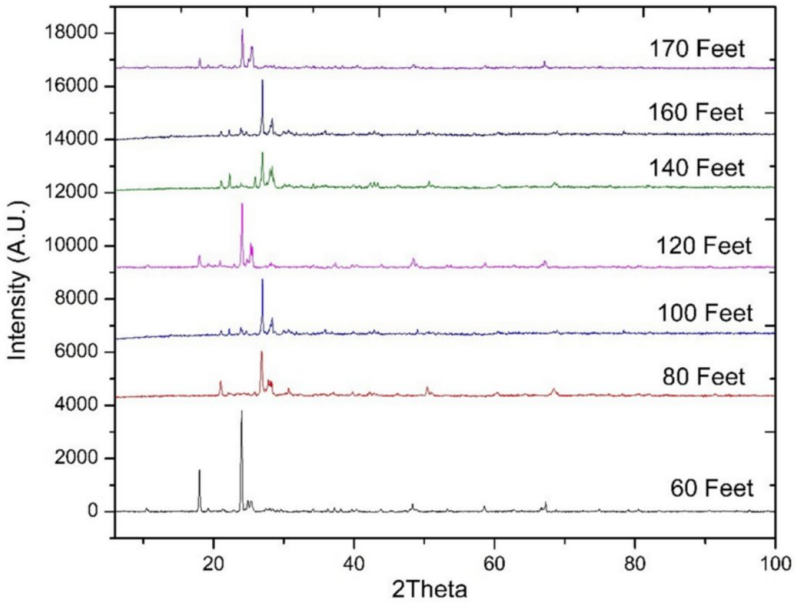

FIGURE 3: Depthwise X-ray Diffraction spectra of rock samples

The X-ray diffractograms confirm the presence of minerals such as quartz, orthoclase, hematite, bauxite, aragonite, microcline, augite, and goethite. Quartz, after feldspars, is the second most abundant mineral in the Earth's crust. Due to its resistance to weathering, quartz is often one of the last minerals to decompose. Quartz particles, typically sand- or gravel-sized, form the structural framework of soil, allowing water to move through soil pores. Soils with high sand content generally exhibit better water permeability but retain less plant-available water compared to clay-rich soils. Dissolved silica from quartz can also influence soil composition and behavior.

One limitation of quartz-rich soils is their deficiency in essential nutrients required for plant growth, as they primarily consist of silicon and oxygen. In contrast, feldspars provide significant nutrients, including calcium, magnesium, and potassium, which are crucial for plant development. Pure quartz is generally an unsuitable medium for plant growth, as it contains only trace amounts of iron and silica. Soils dominated by quartz typically support only highly resilient plant species that either extract nutrients from other minerals or rely on atmospheric nutrient deposition.

The majority of our samples-except those collected at 60 (G1), 120 (G4), and 170 (G7) feet-exhibit high quartz concentrations, making them less suitable for plant life. Conversely, the samples from 60, 120, and 170 feet contain a greater proportion of hematite. Hematite, a primary iron ore mineral, contains a high level of iron oxide. Elevated hematite levels in soil contribute to increased iron availability, a critical nutrient for plant metabolism. Higher iron concentrations enhance plant growth, chlorophyll synthesis, and overall vegetation development.

FTIR results

FTIR was used to evaluate the mineralogical composition of the samples collected [23-26]. Consistent FTIR spectra were obtained from the Perumbakkam hill location in Chennai, Tamil Nadu, India. A combined FTIR spectrum is shown in Figure *4*. FTIR spectra of rock samples at different depths, ranging from 60 to 170 feet, are displayed in Figures *5* to 7, corresponding to the wavenumber ranges of 400-800 cm^{-1}, 800-2000 cm^{-1}, and 2000-4000 cm^{-1}, respectively, to better visualize the minor minerals.

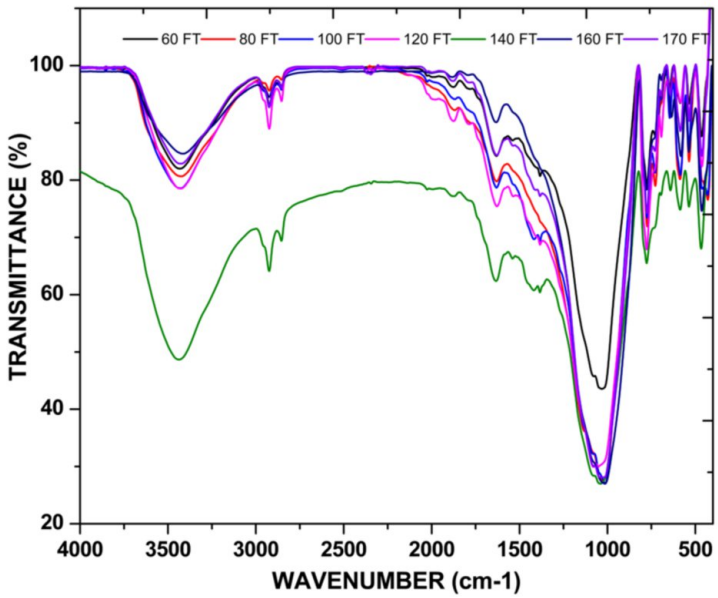

FIGURE 4: FTIR spectra of the depthwise rock samples

FTIR, Fourier Transform Infrared Spectroscopy

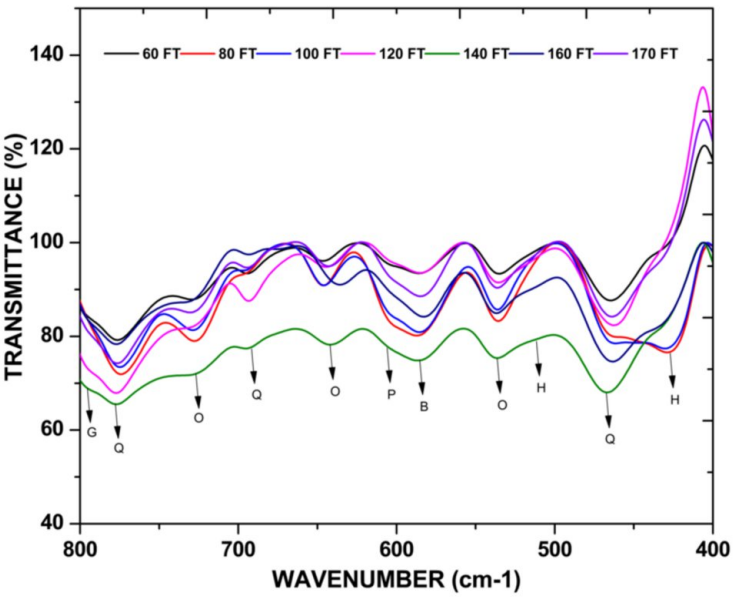

FIGURE 5: FTIR spectra of rock samples (wavenumber 400 to 800 cm-1)

FTIR, Fourier Transform Infrared Spectroscopy

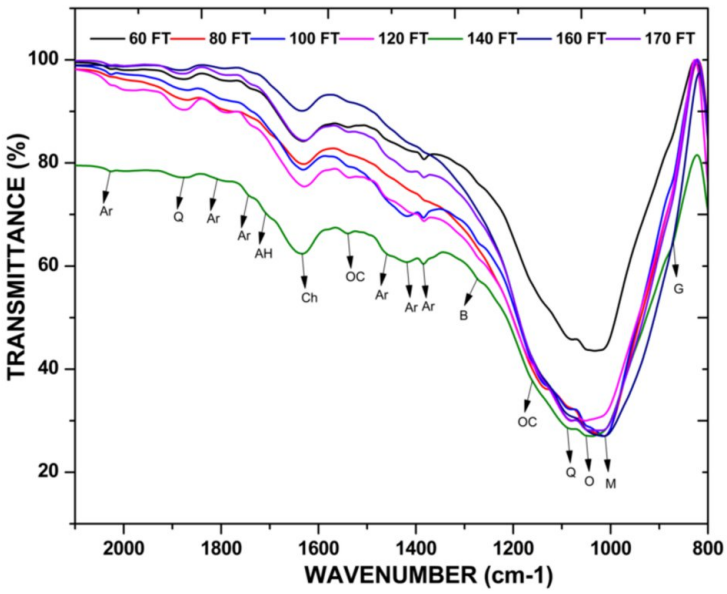

FIGURE 6: FTIR spectra of rock samples (800 to 2000 cm-1)

FTIR, Fourier Transform Infrared Spectroscopy

Observed Frequency (cm^{-1})	Minerals	Remarks	Site Number
420–428	Hematite (α-Fe_2O_3)	Fe-O bending vibrations of hematite	All the sites
440–445	Goethite (α-FeOOH)	Fe-OH bending vibration	100
458–464	Quartz (SiO_2)	Si-O bending modes	All
510-520	Hematite	Fe-O stretching vibrations	100, 140, 160, and 170
533–543	Orthoclase	Fe-O stretching vibrations	All
580–584	Bauxite (mixture of aluminum oxides and hydroxides)	Al-O stretching vibrations	All
600–605	Pyroxenes (Augite, Diopside)	Si-O stretching modes in chain silicates	100, 140, 160, and 170
635–650	Orthoclase	Overlapping metal-oxygen stretches	All
661–666	Hematite	Fe-O stretching vibrations	Only in 170
690–695	Quartz	Si-O bending	All
728–730	Orthoclase or carbonate	Si-O-Al stretching vibrations in feldspars	All
775–780	Quartz	Strong Si-O symmetrical stretching	All
790-800	Goethite	Fe–O–H bending	60, 100, 140
890	Goethite	Fe–O–H bending	60, 100, 140
1009–1015	Microcline	Si(Al)-O stretching vibration	All
1030–1050	Orthoclase and sanidine or microcline	Si(Al)-O and Si-O stretching vibrations (1030) or Si (Al)-O stretching vibrations (1050)	All

1075–1090	Silica (Chalcedony)	Si-O vibrations in amorphous silica or fine-grained quartz (1080) or Si-O stretching Vibration (1090)	All
1125–1140	Orthoclase or sanidine (1025) to Microcline (1040)	Si-O stretching vibration	80, 100, 160, and 170
1170-1175	Quartz	Strong Si-O stretching	60, 80, 120, 140
1270–1275	Organic matter or carbonates	Associated with humic substances or carbonates	All
1380–1385	Aragonite	C-O stretching vibrations	All
1430-1440	Aragonite	C-O stretching vibrations	All
1540–1545	Organic compounds	C=C or C-H bending vibrations (possibly humic materials)	All
1635–1640	Adsorbed water of hematite	O-H bending from water molecules adsorbed on mineral surfaces	All
1760–1780	Carbonates or organic acids	C=O stretching in carbonates or organic matter	All
1882–1886	Quartz	Weak overtone or combination band; typically not strongly diagnostic	All
2380	Atmospheric carbon dioxide (CO_2)	Rather than any specific rock-forming mineral	All
2520	Carbonates	C=O stretching in carbonates or organic matter	All
2854, 2924 & 2960	Organic matter	C-H stretching vibrations in organic compounds	All
3080	Organic compounds or carbonates	Aromatic C-H stretching in organic matter or structural water in carbonates	All
3255–3270	Hydroxyl groups (non-clay)	Broad O-H stretching from in minerals such as goethite and bauxite	All
3280	Goethite	Broad O-H stretching band	All
3420–3440	Absorbed water of hematite	Broad O-H stretching (water content)	All
3610–3625	Bauxite	O-H stretching vibrations (mixture of gibbsite to boehmite)	All

TABLE 2: Observed IR absorption frequencies of rock samples from Perumbakkam

IR, infrared

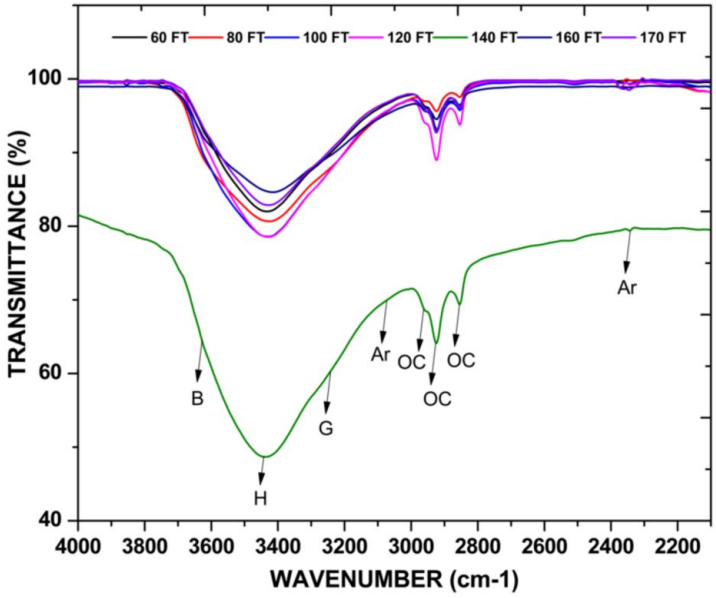

FIGURE 7: FTIR spectra of rock samples (wavenumber 2000 to 4000 cm-1)

FTIR, Fourier Transform Infrared Spectroscopy

The corresponding absorption frequencies are provided in Table *2* for reference. The analysis offered a clear understanding of the sample's structural constituents by examining absorption bands and comparing them with the known mineralogical signatures [27-32]. This approach enabled the identification of key minerals such as iron oxides, clay minerals, silicates (quartz and feldspar), bauxite, pyroxenes, carbonates, and organic matter.

Quartz (SiO_2) and its microcrystalline form, chalcedony, were identified at all sampling sites, with prominent occurrences at depths of 60, 80, 120, and 140 feet. Particularly strong quartz peaks were observed at site 120. Notable Si-O bending vibrations occurred around 458-464 cm^{-1}, while symmetric stretching appeared at 690-695 cm^{-1}, with the most intense peak also recorded at site 120. Additional quartz peaks at 775-780 cm^{-1} and 1170-1175 cm^{-1}, along with an overtone range from 1882 to 1886 cm^{-1}, further confirmed its presence. Chalcedony was detected through Si-O vibrations in the 1075-1090 cm^{-1} range, indicative of amorphous silica or fine-grained quartz. These results suggest the presence of sedimentary deposits or diagenetic alterations in the sampled areas.

Soil minerals interact with IR radiation in ways that depend on factors such as their crystal structure, degree of crystallinity, and extent of weathering [33-37]. Crystallinity is especially important in interpreting these interactions; thus, the crystallinity index of quartz was calculated in this study. At each sampling site, a dominant peak was observed at 775-780 cm^{-1}, and intensity ratios were calculated relative to the nearby 690-695 cm^{-1} band. These ratios, listed in Table *3* and illustrated in Figure *8*, reflect the degree of crystallinity. A higher crystallinity index indicates a more disordered structure, whereas a lower index suggests a more ordered crystalline form [38-40]. In this study, all quartz samples exhibited indices below 1, indicating a relatively well-ordered structure. The crystallinity index of quartz was chosen for analysis because quartz was consistently present in all rock samples. Furthermore, since quartz is the last mineral to crystallize during cooling, its crystallinity index can serve as a proxy for assessing the overall crystalline structure of the rock and other associated minerals.

Site No.	Depth (ft)	Crystallinity Index
G1	60	0.8064
G2	80	0.7230
G3	100	0.7364
G4	120	0.7203
G5	140	0.7894
G6	160	0.8189
G7	170	0.7154

TABLE 3: Crystallinity index of quartz for the peaks at around 778 and 665 cm-1

Feldspar minerals such as Orthoclase, Microcline, and Sanidine were identified at all sites. Their stretching vibration modes Si(Al)-O were observed at 533-543 cm^{-1}, 1009-1015 cm^{-1}, and 1030-1050 cm^{-1}. Group A also showed some additional Si-O stretching peaks at 1125-1140 cm^{-1} that were quite strong at 80 and 100 feet. Metal-oxygen stretches in the range of 635-650 cm^{-1} further confirm the presence of the feldspar component and suggest an igneous or metamorphic source for the parent rocks.

Hematite (α-Fe_2O_3) was present in all locations, with notable amounts at coordinates 100, 140, 160, and 170. This oxide of iron showed Fe-O bending vibrations in the 420-428 cm^{-1} range, with Fe-O stretching occurring at 510-520 cm^{-1}. Site 170 also had an exclusive peak between 661 and 666 cm^{-1}. The broad O-H stretching vibration at 3420-3440 cm^{-1} suggested the presence of weathering or hydration processes on hematite. Additional signals in the 635-650 cm^{-1} region further pointed to these weathering effects.

Goethite (α-FeOOH) was observed at 60, 100, and 140. The site was proved by Fe-OH bending vibrations at 440-445 cm^{-1}, 790-800 cm^{-1}, and 890 cm^{-1}. The presence of secondary iron oxide through hydroxyl ions is brought by weathering processes with a wide O-H band at 3280 cm^{-1}. The analysis detected magnesium-rich chlorite at all sites from O-H bending vibrations from 1635 to 1640 cm^{-1}. The existence of water molecules present in the mineral structure is verified since the O-H stretches exist as broad bands at 3420-3440 cm^{-1}. The chlorite mineral occurs in areas affected by low-grade metamorphic transformations or hydrothermal geological processes.

Bauxite was encountered throughout the samples tested because it contains aluminium associated with hydroxides as well as oxides. The analysis showed that Al-O stretching vibrations appeared at 580-584 cm, and O-H stretching vibrations due to gibbsite and boehmite were at 3610-3625 cm^{-1}. The strongest evidence to prove that the material contained hydroxyl groups was the broad O-H stretching band at 3255-3270 cm^{-1}. The weathering processes impacting the bauxite formation are starting to impact aluminium-rich rocks that occurred during tropical or lateritic soil conditions.

Sites 100, 140, 160 together with 170 contained augite and diopside, while both augite and diopside were noted at these sites. Site listing confirms that Si-O stretching modes at 600-605 cm^{-1}, which belong to the composition of the samples analyzed, are characteristic of carbonate and igneous emplaced metasedimentary rocks. At all research sites, dolostone along with dolomite, was noted as a constituent of carbonates.

Their C-O stretching vibrational modes were recorded at 1380-1385 cm^{-1} and 1430-1440 cm^{-1}, along with additional C=O vibrational modes at 1760-1780 cm^{-1} and 2520 cm^{-1}. The presence of carbonates is validated by a peak at 3080 cm^{-1}, either of sedimentary origin or due to secondary mineralization [41].

Organic matter and hydroxyl groups were observed across all locations, with C-H and C=C bending vibrations recorded at 1270-1275 cm^{-1}, 1540-1545 cm^{-1}, 2854 cm^{-1}, 2924 cm^{-1}, and 2960 cm^{-1}. The presence of organic compounds suggests biological activity or organic matter incorporation within the sediments. Atmospheric CO_2 absorption at 2380 cm^{-1} indicated interactions between minerals and environmental gases [42].

Soil microbial diversity and its role in soil health

Soil microbial diversity represents the essential operational aspect of soil biota since it underpins earth sustainability. Soil health determination depends on microorganism analysis since these living organisms can adjust to environmental conditions. Soil quality assessment relies on changes in microbial numbers and operational levels to determine ecosystem changes.

The measured bacterial population levels across the study area where counts ranged from 1000 to 2300 CFU/ml (Table *4*). Deployment G7 registered the highest density of bacteria because a total of 23 bacterial colonies were observed there. The elevated humidity at 170 cm in G7 promotes bacterial growth, which contributes to these higher microbial numbers. Sites G3 and G6 yielded the minimum number of bacterial colonies as their counts reached only 10.

Site No.	Depth (ft)	PH	Number of colonies counted	CFU/ml
G1	60	7.15	22	2200
G2	80	7.45	12	1200
G3	100	7.50	10	1000
G4	120	7.25	19	1900
G5	140	7.35	11	1100
G6	160	7.40	10	1000
G7	170	7.26	23	2300

TABLE 4: Colony Forming Units and pH for various sampling sites

Soil and rock environments show various advantages because bacteria exist within these systems. Microorganisms perform essential functions by breaking down organic substances to produce available forms of essential nutrients, including nitrogen, phosphorus, and potassium for plant uses. Soil microbial agents work through their activities to develop soil aggregates while improving both infiltration and air movement, and root system growth [43]. The beneficial microbes help defeat plant diseases by challenging damaging microorganisms, which leads to improved root disease protection and enhanced plant adaptability.

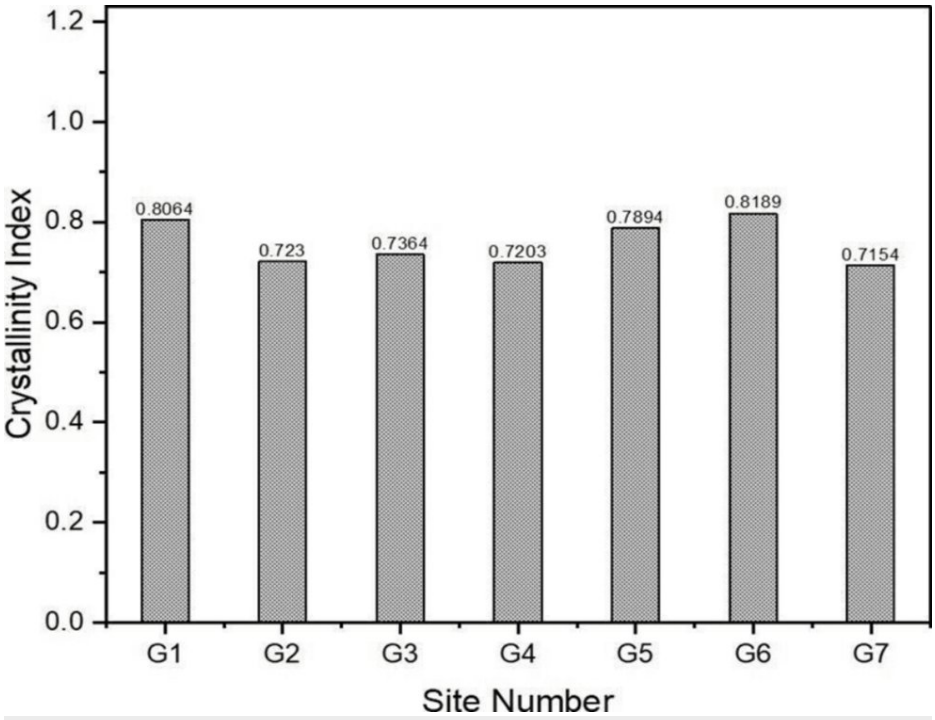

FIGURE 8: Depth wise Crystallinity index of Quartz

The large microbial abundance at G7 might be due to the presence of a higher percentage of hematite in this region when compared to other zones. According to Basinskiiron et al. [44,45], oxides, including hematite, can catalyze the conversion of organic phosphorus into inorganic phosphate, at rates comparable to those of enzymatic reactions, thereby enhancing the availability of phosphorus to plants within the soil. Reference: unraveling iron oxides as abiotic catalysts of organic phosphorus recycling in soil and sediment matrices. This makes this zone an excellent agricultural area because deep-rooted crops flourish from intensified microbial engagements within the soil.

Influence of soil pH on microbial composition and plant growth

The pH value of soil controls microbial community formation by directly affecting microorganism physiological activities. The composition of bacteria in soil depends on the soil properties that relate to its pH levels [46]. Therefore, environmental shifts in pH affect bacterial diversity directly and indirectly. The study area showed a pH range between 7.15 and 7.50. The measurement location at G3 (100 feet) yielded the highest pH value of 7.50 while G1 (60 feet) showed the lowest measurement of 7.15. Plant growth benefits from the neutral to slightly alkaline category at this pH range, which makes the soil ideal for development. Plants succeed best at these pH values because all necessary nutrients can be easily absorbed [47].

A soil pH value above 7.5 causes essential nutrients such as phosphorus, together with manganese and iron to become unavailable, which impairs plant development. Soil conditions in Perumbakkam provide perfect conditions for both agricultural operations and plant farming because the pH levels in the area remain within the accepted ranges.

Conclusions

The present investigation of Perumbakkam hill offers detailed insights into its mineralogical composition and geological structure, emphasizing its potential for sustainable land utilization and georesource development. Integrated XRD and FTIR analyses confirm that quartz, feldspar (orthoclase and microcline), bauxite, and hematite dominate the mineralogical profile. These minerals, shaped by natural weathering and depositional processes, display variations in crystallinity and structural integrity, which enhance the physical robustness and chemical resilience of the terrain, qualities well-suited for applications in construction and mineral-based industries. The analysis of microbial distribution across soil depths revealed notable biological richness, with the highest bacterial colony count (2300 CFU/ml) recorded at 170 feet. This depth also corresponded to increased hematite concentration, suggesting a possible link between mineral composition and microbial abundance. Soil pH analysis showed a maximum value of 7.50, indicative of a slightly alkaline environment that promotes microbial activity and nutrient availability. Such conditions are ideal for supporting deep-rooted, nutrient-demanding crops, reinforcing the region's agricultural suitability.

In conclusion, this study enhances our understanding of the geological and ecological interdependencies at Perumbakkam hill and affirms its suitability for agriculture, environmental conservation, and mineral resource exploitation. Future interdisciplinary research combining detailed mineralogical assessments with microbial ecology and sustainable land-use planning will further unlock the scientific and economic potential of this landscape.

Additional Information

Author Contributions

All authors have reviewed the final version to be published and agreed to be accountable for all aspects of the work.

Concept and design: Murugesan Sugumaran, Gayathri Arun

Acquisition, analysis, or interpretation of data: Murugesan Sugumaran, Gayathri Arun

Drafting of the manuscript: Murugesan Sugumaran, Gayathri Arun

Critical review of the manuscript for important intellectual content: Murugesan Sugumaran, Gayathri Arun

Supervision: Murugesan Sugumaran

Disclosures

Human subjects: All authors have confirmed that this study did not involve human participants or tissue.
Animal subjects: All authors have confirmed that this study did not involve animal subjects or tissue.

Conflicts of interest: In compliance with the ICMJE uniform disclosure form, all authors declare the following: **Payment/services info:** All authors have declared that no financial support was received from any organization for the submitted work. **Financial relationships:** All authors have declared that they have no financial relationships at present or within the previous three years with any organizations that might have an interest in the submitted work. **Other relationships:** All authors have declared that there are no other relationships or activities that could appear to have influenced the submitted work.

References

1. Zandomeneghi D, Voltolini M, Mancini L, Brun F, Dreossi D, Polacci M: Quantitative analysis of X-ray microtomography images of geomaterials: Application to volcanic rocks. Geosphere. 2010, 6:793-804. 10.1130/ges00561.1
2. Setiawan MR, Iqbal M, Siregar RN: Mineral analysis in rocks using XRD and petrography. Journal of Science and Applicative Technology. 2019, 2:10.35472/281459
3. Rahman T, Maxim L, Yihuai Z, Ahmed B, Stefan I: Influence of rock microstructure on its electrical properties: an analysis using X-ray microcomputed tomography. Energy Procedia. 2017, 114:5023-31. 10.1016/j.egypro.2017.03.1651
4. Sabri MM: Chemical and structural analysis of rocks using X-ray fluorescence and X-ray diffraction techniques. ARO-The Scientific Journal of Koya University. 2020, 8:79-87. 10.14500/aro.10643
5. Tamilarasi A, Sathish V, Manigandan S, Chandrasekaran A: Data on minerals and crystallinity index of quartz in rock samples collected from Paleolithic archaeological site of Attirampakkam, Tamil Nadu. Data in Brief. 2021, 39:107571. 10.1016/j.dib.2021.107571
6. Abbady A, Ahmed NK, El-Arabi AM, Michel R, El Kamel AH, Abbady AGE: Estimation of radiation hazard indices from natural radioactivity of some rocks. Nuclear Science and Techniques. 2006, 17:118-22. 10.1016/s1001-8042(06)60023-7
7. Sánchez-Sánchez A, Cerdán M, Jordá JD: Characterization of soil mineralogy by FTIR: application to the analysis of mineralogical changes in soils affected by vegetation patches. Plant and Soil. 2019, 439:447-58. 10.1007/s11104-019-04061-6
8. Al-Ghamdi AH: X-ray diffraction and gamma-ray analysis of rock samples from Haradh Region in Saudi Arabia. Journal of Radiation Research and Applied Sciences. 2019, 12:87-92. 10.1080/16878507.2019.1594142
9. Hillier S: Accurate quantitative analysis of clay and other minerals in sandstones by XRD: comparison of a Rietveld and a reference intensity ratio (RIR) method and the importance of sample preparation. Clay Minerals. 2000, 35:291-302. 10.1180/000985500546666
10. India Meteorological Department (IMD): Annual Climate Report. (2021). Accessed: May 15, 2021: https://metnet.imd.gov.in/docs/imdnews/.
11. Niemela J: Ecology and urban planning. Biodiversity & Conservation. 1999, 8:119-31.
12. Reddy CS, Jha CS, Dadhwal VK: Spatial dynamics of deforestation and forest fragmentation (1930-2013) in Eastern Ghats, India. The International Archives of the Photogrammetry Remote Sensing and Spatial Information Sciences. 2014, XL-8:637-44. 10.5194/isprsarchives-xl-8-637-2014
13. Kosmulski M, Maczka E, Jartych E, Rosenholm JB: Synthesis and characterization of goethite and goethite-hematite composite: experimental study and literature survey. Advances in Colloid and Interface Science. 2003, 103:57-76.
14. Pandey V, Gautam P, Singh AP: Study of microbial count in soil under different land use systems in a mollisol. International Journal of Current Microbiology and Applied Sciences. 2019, 8:16-21. 10.20546/ijcmas.2019.801.002
15. Xiong R, He X, Gao N, Li Q, Qiu Z, Hou Y, Shen W: Soil pH amendment alters the abundance, diversity, and composition of microbial communities in two contrasting agricultural soils. Microbiology Spectrum. 2024, 12:e04165-23. 10.1128/spectrum.04165-23
16. Hamed H, Hale W, Stern B: X-Ray diffraction to determine the mineralogy in soil samples in the UK. International Journal of Engineering Applied Sciences and Technology. 2021, 5:91-98.
17. Kemp TJ, Alcock NW: 100 years of X-ray crystallography. Science Progress. 2017, 100:25-44. 10.3184/003685017x14858694684395
18. Ramasamy V, Pachamuthu R, Ponnusamy V: Depth wise analysis of recently excavated Vellar river sediments through FTIR and XRD studies. Indian Journal of Physics. 2009, 83:1295-308. 10.1007/s12648-009-0110-3
19. Chipera SJ, Bish DL: Baseline studies of the clay minerals society source clays: Powder X-ray diffraction analyses. Clays and Clay Minerals. 2001, 49:398-409. 10.1346/ccmn.2001.0490507
20. Chung FH: Quantitative interpretation of X-ray diffraction patterns of mixtures. II. Adiabatic principle of X-ray diffraction analysis of mixtures. Journal of Applied Crystallography. 1974, 7:526-31. 10.1107/s0021889874010387
21. Lu L, Sahajwalla V, Kong C, Harris D: Quantitative X-ray diffraction analysis and its application to various coals. Carbon. 2001, 39:1821-833. 10.1016/s0008-6223(00)00318-3
22. Karine F, Emmanuel G, Michel A, Eric M, Lorenzo S, Patricia B, Yves-Michel F: Characterization of soil particles by X-ray diffraction (XRD), X-ray photoelectron spectroscopy (XPS), electron paramagnetic resonance (EPR) and transmission electron microscopy (TEM). Agronomy for Sustainable Development. 2005, 25:345-53. 10.1051/agro:2005037
23. Madejova J: FTIR techniques in clay mineral studies. Vibrational Spectroscopy. 2003, 31:1-10. 10.1016/s0924-2031(02)00065-6
24. Packialakshmi S, Ambujam NK: The peri-urban to urban groundwater transfer and its societal implications in Chennai, south India - A case study. Indian Journal of Agricultural Research. 2017, 51:135-41. 10.18805/ijare.v0iof.7639
25. Castellini E, Berthold C, Malferrari D, Bernini F: Sodium hexametaphosphate interaction with 2:1 clay minerals illite and montmorillonite. Applied Clay Science. 2013, 83-84:162-70. 10.1016/j.clay.2013.08.031
26. Ellies A, Ramirez C, MacDonald R: Organic matter and wetting capacity distribution in aggregates of Chilean soils. CATENA. 2005, 59:69-78. 10.1016/j.catena.2004.05.005
27. Chaparro MAE, Sinito AM, Ramasamy V, Marinelli C, Chaparro MAE, Mullainathan S, Murugesan S: Magnetic

measurements and pollutants of sediments from Cauvery and Palaru River, India. Environmental Geology. 2008, 56:425-37. 10.1007/s00254-007-1180-1

28. Bender SF, Wagg C, van der Heijden MGA: An underground revolution: biodiversity and soil ecological engineering for agricultural sustainability. Trends in Ecology & Evolution. 2016, 31:440-52. 10.1016/j.tree.2016.02.016
29. Murugesan S: Identification of minor minerals in river sediments through FTIR study - A new approach. Pollution Research. 2020, 39:156-60.
30. Ramasamy V, Murugesan S, Mullainathan S: Characterization of minerals and distribution of quartz in Cauvery River sediments - A FTIR study. Bulletin of Pure and Applied Sciences. 2004, 23F(1-2):1-11.
31. Calderón F, Haddix M, Conant R, Magrini-Bair K, Paul E: Diffuse-reflectance FT-MIR as a method of characterizing changes in soil organic matter. Soil Science Society of America Journal. 2013, 77:1591-600. 10.2136/sssaj2013.04.0131
32. Haberhauer G, Gerzabek MH: Drift and transmission FT-IR spectroscopy of forest soils: an approach to determine decomposition processes of forest litter. Vibrational Spectroscopy. 1999, 19:413-17. 10.1016/s0924-2031(98)00046-0
33. Ramasamy V, Anandalakshmi K, Ponnusamy V: Rapid determination of quartz and characterization of feldspars in rock using FTIR. Indian Journal of Physics . 2003, 77:347-52.
34. Farias TMB, Gennari RF, Chubaci JFD, Watanabe S: FTIR spectra and TL properties of quartz annealed at high temperatures. Physics Procedia. 2009, 2:493-96. 10.1016/j.phpro.2009.07.034
35. Fahad M, Ali S, Shah KH, Shahzad A, Abrar M: Quantitative elemental analysis of high silica bauxite using calibration-free laser-induced breakdown spectroscopy. Applied Optics. 2019, 58:7588-596. 10.1364/ao.58.007588
36. Han W, Wang F, Zhang L, Zhao H, Zheng Y, Sun R, Meng L: Variations of soil bacterial community and denitrifier abundance with depth under different land-use types. Journal of Soils and Sediments. 2023, 23:1889-900. 10.1007/s11368-023-03428-8
37. Ellerbrock RH, Stein M, Schaller J: Comparing silicon mineral species of different crystallinity using Fourier transform infrared spectroscopy. Frontiers in Environmental Chemistry. 2024, 5:1462678. 10.3389/fenvc.2024.1462678
38. Chen Y, Zou C, Mastalerz M, Hu S, Gasaway C, Tao X: Applications of Micro-Fourier Transform Infrared Spectroscopy (FTIR) in the geological sciences—a review. International Journal of Molecular Sciences. 2015, 16:30223-250. 10.3390/ijms161226227
39. Gotze J, Pan Y, Muller A: Mineralogy and mineral chemistry of quartz: A review. Mineralogical Magazine. 2021, 85:639-64.
40. Durgut E, Cinar M, Terzi M, Kursun Unver I, Yildirim Y, Ozdemir O: Evaluation of different dispersants on the dispersion/sedimentation behavior of halloysite, kaolinite, and quartz suspensions in the enrichment of halloysite ore by mechanical dispersion. Minerals. 2022, 12:1426. 10.3390/min12111426
41. Saikia BJ: Spectroscopic estimation of geometrical structure elucidation in natural SiO2 crystal. Journal of Materials Physics and Chemistry. 2014, 2:28-33. 10.12691/jmpc-2-2-3
42. Ozgen S, Çilek EC: Effects of some cations to the surface properties of silicates (feldspar and quartz). University Journal of the Institute Science and Technology. 2012, 28:116-21.
43. Yukselen-Aksoy Y, Kaya A: Zeta potential of kaolinite in the presence of alkali, alkaline earth and hydrolyzable metal ions. Water Air & Soil Pollution. 2003, 145:155-68. 10.1023/a:1023684213383
44. Basinski JJ, Bone SE, Klein AR, et al.: Unraveling iron oxides as abiotic catalysts of organic phosphorus recycling in soil and sediment matrices. Nature Communications. 2024, 15:1-14. 10.1038/s41467-024-47931-z
45. Cui H, Zhang X, Wu Q, et al.: Hematite enhances the immobilization of copper, cadmium and phosphorus in soil amended with hydroxyapatite under flooded conditions. The Science of The Total Environment. 2020, 708:134590. 10.1016/j.scitotenv.2019.134590
46. Ye WM, Qi ZY, Chen B, Xie J, Huang Y, Lu YR, Cui YJ: Mechanism of cultivation soil degradation in rocky desertification areas under dry/wet cycles. Environmental Earth Sciences. 2010, 64:269-76. 10.1007/s12665-010-0846-2
47. Baron MA, Stalder R, Konzett J, Hauzenberger CA: OH-point defects in quartz in B- and Li-bearing systems and their application to pegmatites. Physics and Chemistry of Minerals. 2014, 42:53-62. 10.1007/s00269-014-0699-4